Article

Friedel Oscillations and He-He Interactions in Mo

Xuepeng Shen [1], Enzhi Liang [2], Qian Zhan [3], Wei Wang [4] and Wen Tong Geng [5],*

1 Research Department, Ningxia Normal University, Guyuan 756000, China
2 Shenzhen Menpad Technology Group Company Limited, Shenzhen 518000, China; maxliang@menpad.com
3 School of Materials Science and Engineering, University of Science and Technology Beijing, Beijing 100083, China
4 School of Electrical and Information Engineering, North Minzu University, Yinchuan 750021, China
5 Department of Physics, Zhejiang Normal University, Jinhua 321004, China
* Correspondence: wtgeng@zjnu.edu.cn

Abstract: Helium ions implanted into metals can form ordered bubbles that are isomorphic to the host lattice. While long-range elastic interactions are generally believed to drive bubble superlattice formation, the interactions between individual helium solutes are not yet fully understood. Our first-principles calculations reveal that in molybdenum, Friedel oscillations induced by individual helium atoms generate potential barriers and wells that influence helium pairing and clustering at short He-He distances. These repulsive and attractive interactions at high concentrations provide thermodynamic driving forces that align randomly distributed helium atoms into Mo-He superlattices. Friedel oscillations may have broad impacts on solute–solute interactions in alloys.

Keywords: Friedel oscillations; helium irradiation; molybdenum; first-principles; solute–solute interactions

1. Introduction

When a metal is irradiated with neutrons or heavier particles at elevated temperatures, abundant vacancies emerge and agglomerate into microcavities that are known as voids or bubbles if they are filled with gas. It was discovered by Evans half a century ago that such voids in Mo form a nearly perfect body-centered cubic (bcc) lattice structure isomorphic to the matrix crystal [1]. Soon after, bcc superlattices of He bubbles were also found in Mo [2]. In addition, extensive investigations revealed the self-organization of isomorphic superlattices of voids and He bubbles under high-dose irradiation conditions in many other metals with bcc, face-centered cubic (fcc), or close-packed hexagonal (hcp) lattices [3–5]. Understanding the physical origin of this nanostructure self-organization is important in fundamental condensed matter physics and crucial from a technological perspective because knowledge of the dependence of a microstructure on the irradiation and material conditions can be helpful in the design of radiation-resistant materials in nuclear reactors.

Various models have been proposed to explain the formation of void and bubble superlattices. The early models proposed by Tewary and Bullough [6], Stoneham [7], and Wills [8], which consider only elastic interactions between voids, can reproduce the existence of an energy minimum at a particular void–void distance and give somewhat reasonable ratios between this distance and the void radius in Mo; however, the dynamic ordering process is totally unknown. Other authors have explored the concept of phase transitions in nonequilibrium conditions [9], the idea of the anisotropic diffusion of self-interstitial-atoms [4,10], and the theory of non-linear dynamics for dissipative systems [11]. More recent models take into account both elasticity and dynamic diffusion processes based on the phase-field method, and obtain better agreement with experimental observations on the growth and ordering of voids and bubbles in different metals [12–14].

It has been well established that in the early stages of the superlattice formation, small voids or bubbles are distributed randomly in the host metal [4,11,14,15]. It appears

that the initially disordered small voids move around in a Brownian motion until a small group of them happen to reach a correct configuration allowing them to nucleate into a superlattice with an appropriate lattice parameter which minimizes the free energy. However, it must be stressed that fundamental information about the stability of individual solute He atoms at the initial stage of bubble formation is still missing. Due to the strong He–vacancy binding [16,17] and the abundance of vacancies under irradiation conditions, the implanted He atoms may immediately take substitutional positions, presumably in a disordered manner. First-principles calculations demonstrate that He is more stable at a substitutional site than at an interstitial site in Mo. Since the $1s$ electrons in a He atom are at a deep level and paired, He experiences Pauli repulsion in electron gas and cannot form a chemical bond with any other elements [18]. Therefore, substitutional He atoms have strong tendencies to first merge into clusters and then into bubbles to reduce the He–matrix interfacial energy. Thus, an important question arises: do individual solute He atoms have the tendency to stay away from each other before coalescing into clusters? If yes, why? Apparently, the underlying repulsive force plays a crucial role in the formation of dense and randomly positioned small bubbles before they merge and reassemble into a periodic array of larger bubbles.

Such a He-He repulsive force should have a long-range nature since the two atoms are separated by at least one host atom in the matrix lattice before forming a He-He pair. One might be tempted to assume that the force originates from the elastic interaction between point defects. However, it is known from first-principles calculations that substitutional He atoms in W, which has a lattice constant very close to that of Mo, has an effective atomic size nearly the same as that of W atoms (difference in radius of < 0.01Å) [19]. This means that the elastic interactions should be very weak between individual He atoms before they agglomerate into bubbles. In trying to tackle this puzzle, we can recall two facts: (i) He as an impurity will lead to Friedel oscillations [20] in the electron density in the host metal, [21] and (ii) He almost always prefers a low-electron-density region in metals [18]. Recognizing these two features inspires us to conjecture that it might be the effect of Friedel oscillations that give rise to the sizable long-range He-He interactions in metals.

2. Model and Computation

To verify this hypothesis, we employed first-principles density functional theory (DFT) calculations to evaluate the He-He interactions in Mo at different concentrations in terms of solution energy variation. To keep the computation affordable, individual substitutional He atoms were put into symmetric lattice sites in Mo, forming a superlattice based the original lattice of Mo itself. By itself, the superlattice composed of implanted He atoms is a simple cubic, bcc, or fcc structure. Note that a substitutional He atom can be viewed as a combination of an He atom and a vacancy, which is superabundant under irradiation. These models are illustrated in Figure 1, taking (2 × 2 × 2) supercells as an example.
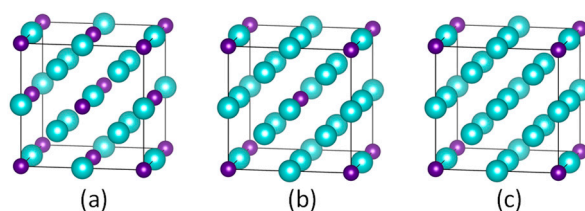

(a)   (b)   (c)

Figure 1. Computational model for ordered substitutional He (small spheres) in Mo (large spheres), forming an fcc (**a**), bcc (**b**), or simple cubic (**c**) superlattice. The (2 × 2 × 2) host supercells are taken as an example.

We performed DFT calculations using the Vienna Ab initio Simulation Package [22]. The electron–ion interaction was treated using the projector augmented wave (PAW) method [23]. The exchange correlation between electrons was described with a generalized gradient approximation (GGA) in Perdew–Burke–Ernzerhof (PBE) form [24]. There

is DFT evidence that the PBE functional describes well the He-metal interactions and the inclusion of van der Waals correction yield only negligible changes [25]. We used an energy cutoff of 500 eV for the plane wave basis set for all systems to ensure equal footing. To calculate the solution energies for ordered He at different concentrations, we employed supercells ranging from ($2 \times 2 \times 2$) to ($7 \times 7 \times 7$) composed of bcc Mo. We modelled concentrations ranging from 25 at% to 0.6 at% for an array of He atoms in an fcc superlattice and concentrations ranging from 12.5 at% to 0.3 at% for such an array in a bcc superlattice. For a simple cubic He superlattice, we included the ($1 \times 1 \times 1$) Mo cell so that the He concentration varied from 50 at% to 0.15 at%. The Brillouin zone integration was performed within the Monkhorst–Pack scheme using a dense k mesh composed of ($24 \times 24 \times 24$), ($12 \times 12 \times 12$), ($8 \times 8 \times 8$), ($6 \times 6 \times 6$), ($5 \times 5 \times 5$), and/or ($4 \times 4 \times 4$) Mo supercells, respectively. To investigate the short-range He-He interactions at low concentrations, we put two He atoms in a ($7 \times 7 \times 7$) supercell along the <111> direction and calculated the change in pairing energy when varying the He-He distance. For all supercells, we started from the configurations in which He took substitutional positions and all the matrix atoms were in prefect bulk sites. Then, we optimized both internal coordinates and supercell dimensions. The energy relaxation for each supercell was continued until the total energies were converged to less than 1×10^{-4} eV/cell. We noted that the total energy of the initial configuration was the one before the He-He elastic interactions took effect.

3. Results and Discussion

The solution energy of He in Mo, $\Delta H_s(\text{He})$, can be obtained via

$$\Delta H_s(\text{He}) = \frac{1}{n}[E(\text{Mo}_{2m^3-n}\text{He}_n) - (1 - \frac{n}{2m^3}) \times E(\text{Mo}_{2m^3}) - nE(\text{He})], \tag{1}$$

where $E(\text{Mo}_{2m^3-n}\text{He}_n)$ is the total energy of the ($m \times m \times m$) supercell containing 2 m^3-n Mo and n He atoms, $E(\text{Mo}_{2m^3})$ is the total energy of the clean ($m \times m \times m$), $E(\text{He})$ is the total energy of an isolated He atom, which is set to zero, and n = 4, 2, or 1 for an fcc, bcc, or simple cubic superlattice of He in Mo. We display in Figure 2 the calculated solution energy of substitutional He atoms in Mo. For the case of isomorphic distribution, we also show the solution energy of He in *frozen* configurations (open symbols), in addition to that in fully relaxed configurations (solid symbols). By *frozen*, we mean all atoms in a supercell are in the ideal lattice sites, and the contribution of He-He elastic interactions to the total energy is non-existent.
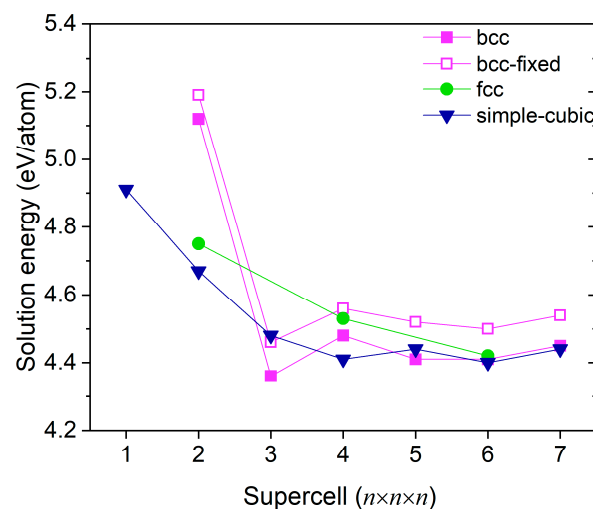

Figure 2. The solution energy of substitutional He in Mo supercells. The concentration of He is $1/n^3$, $2/n^3$, and $4/n^3$ for simple cubic, bcc, and fcc He superlattices.

One striking feature shown in Figure 2 is that the solution energy of He takes the highest value in the smallest supercell. This indicates that before collectively merging into clusters upon which there is significant energy release, He atoms experience a repulsion from each other at high concentrations. Such a barrier changes very little from 0.76 to 0.73 eV per He atom upon geometry optimization when elastic interactions take effect. It can therefore be concluded there must be a driving force other than He-He elastic interactions responsible for the oscillations in the solution energy relative to the concentration. Another interesting finding is that the solution energy of He reaches a local minimum before reaching the barrier in the isomorphic bcc structure. By comparison, the solution energy of a non-isomorphic array of He generally increases from low to high. The nearest-neighbor He-Mo distance in the configuration of one He in $(7 \times 7 \times 7)$ Mo supercell is 2.728 Å, which is only 0.005 Å larger than the Mo-Mo bond length in bulk, and hence a marginal size effect. It is for this reason that the difference in the solution energy of He in the *frozen* supercells and the fully optimized supercells does not vary remarkably with concentration, indicating that the He-He elastic interactions are very weak. It is noteworthy that in the absence of elastic interactions, Friedel oscillations alone can also give rise to rearrangement of atomic positions, as evidenced in the relaxation of free surfaces [26].

We have also studied He-He interactions at short ranges in the case of low concentrations by evaluating the solution energy of a He pair. We have varied the He-He distance in $(5 \times 5 \times 5)$, $(6 \times 6 \times 6)$, $(7 \times 7 \times 7)$, and $(8 \times 8 \times 8)$ Mo supercells embedded with two substitutional He atoms sitting along the <111> direction. The corresponding He concentrations in these settings are 1/125 (0.8%), 1/216 (0.5%), 1/343 (0.3%), and 1/512 (0.2%), respectively. The calculated solution energy per He atom in each supercell as a function of He-He distance is shown in Figure 3. Very similar to the results displayed in Figure 2 (solid squares), we see clear oscillations of the He-He interactions at low concentrations. The magnitude of oscillation is smaller than that in the high concentration case, as the number of nearest He neighbors is only two, while it is eight in the former case. To better illustrate a specific He-He interaction, we display it in the form of He-He interatomic potential in the $(8 \times 8 \times 8)$ Mo supercell, as shown in Figure 4. Note that the potential is assumed, as an approximation, to fade to zero at a He-He distance of seven times the Mo-Mo bond length. Such an interatomic potential can be fairly fitted as $V(r) = 0.8 \times \cos(2.5r - 1.25) \times \frac{1}{r^3}$, in which r is the He-He distance. Clearly, this equation is very different from that in a vacuum where there are no oscillations [19].
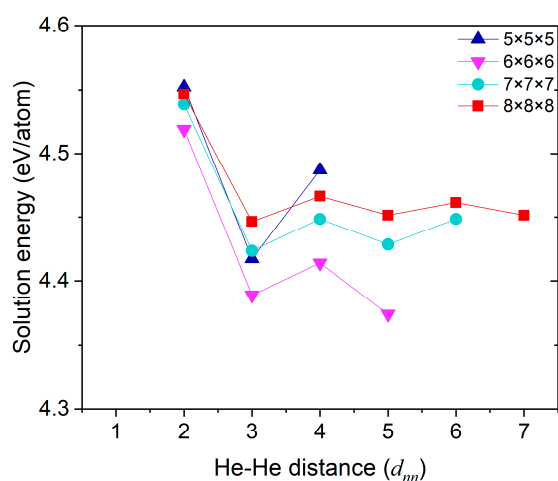

Figure 3. The solution energy (eV/atom) of a He pair in <111> direction in a $(m \times m \times m)$ Mo supercell ($m = 5, 6, 7, 8$) at various Mo-Mo distances (at the scale of the Mo-Mo bond length d_{nn}).
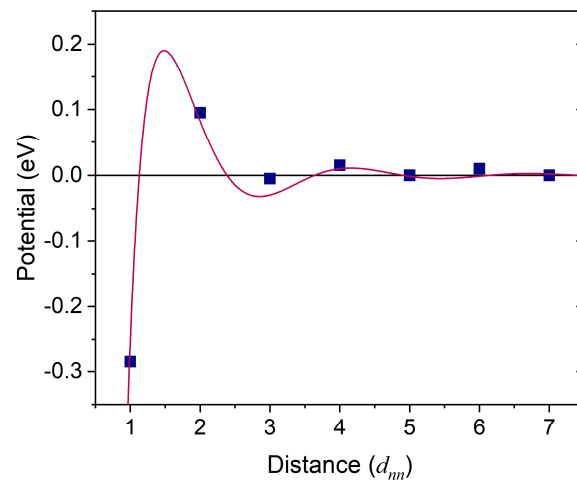
Figure 4. The DFT-calculated (squares) and curve fitting He-He interatomic potential along the <111> direction in Mo in a (8 × 8 × 8) supercell. Distance is in the scale of the Mo-Mo bond length d_{nn} = 2.723 Å.

The fitted He-He interatomic potential reminds us of the phenomenon called Friedel oscillation. Friedel oscillations are spatial modulations of the electron density in a metal whenever a local disturbance occurs [20]. Static Friedel oscillations have the form of a standing wave perturbation, and they disappear with increasing distance from the disturbance. Near a point impurity, the relative change of electron density, $\frac{\Delta\rho}{\rho}$, decays with distance, r, in a jellium model as [21]

$$\frac{\Delta\rho}{\rho} \sim \cos\left(2k_f r - \varphi\right) \times \frac{1}{r^3}, \tag{2}$$

where k_f is the Fermi wavevector of the electron gas in the host metal and φ is the phase shift accounting for the electron transfer between the impurity and the host. The discrete nature of the crystal lattice means that Friedel oscillations are orientation-dependent in real metals, following the Fermi wavevector variation [27]. Keeping in mind that He prefers a low-electron-density environment when substituting for a matrix atom, we are more interested in the electron density variation along atomic chains containing the He atom. We have chosen three low-index directions, <100>, <110>, and <111>, and calculated the relative change in charge density along these three directions upon replacing one Mo atom with an He atom.

Figure 5 displays the Friedel oscillations induced by one He atom in a (7 × 7 × 7) Mo supercell. The inset is a closeup of a narrower distance range. We point out that the Friedel oscillations are the relative electron density change in the metal with the introduction of an impurity. Thus, they do not impact the impurity atom, especially in the core region. For this reason, we start the plot at r = 0.2 d_{nn}, where d_{nn} is the nearest-neighbor Mo-Mo distance. Clearly, oscillations in the <111> direction are the strongest, and those in the <110> direction, which has the largest Mo-Mo distance, is the weakest, indicating that chemical bonds have stronger responses than interstitial itinerant electrons. Apparently, the first Mo atom along <111>, occupying the region $0.5 < r < 1.5$, loses electrons, the second Mo gains electrons, and the third also lose electrons in an oscillatory manner. The change in electron density beyond the third Mo is negligible. Along <100>, the first Mo atom, occupying the region $0.65 < r < 1.65$ lose electrons like that in the <111> direction, the second Mo $1.8 < r < 2.8$ gains electrons with a much smaller magnitude, and the third Mo $2.95 < r < 3.95$ undergoes a very slight electron loss. As for <110>, the first Mo $1.1 < r < 2.1$ gains electrons, in accordance with the fact that its distance to He is 1.6 d_{nn}, which is much larger than the nearest neighbor. All these features effectively explain the results of the calculated solution energies presented in Figures 2 and 3 and provide a

clear physical picture of the appearance of the high energy state around $r = 2d_{nn}$ and the low energy state around $r = 3d_{nn}$ in the <111> direction. This finding implies that in the agglomeration process of implanted He atoms, there will be a remarkable potential barrier (0.7 eV) before the occurrence of He clustering, and there is a shallow potential well right before that barrier (0.1 eV).
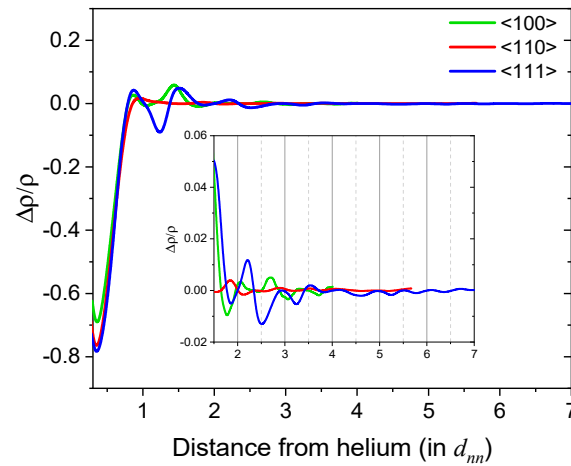

Figure 5. The Friedel oscillations of charge density along the <100>, <110>, and <111> directions in Mo upon replacing one Mo with a helium in a $(7 \times 7 \times 7)$ supercell. Distance from the He atom is at the scale of the Mo-Mo bond length $d_{nn} = 2.723$ Å.

To gain deeper insights into the oscillations in the charge density, we have calculated the local density of states (LDOS) of Mo atoms at varying distances from the embedded He along the <111> direction in the $(7 \times 7 \times 7)$ supercell. It is seen clearly in Figure 6 that the LDOS of a certain Mo atom changes remarkably with the Mo-He distance i.e., the number of matrix atoms in between the two, and the perturbation effect of He on the electronic structure has a long-range nature. In the inset, we show the calculated LDOSs of Mo atoms at the Fermi energy level, which makes the major contribution to the electron density in the interstitial region. It is found that with increasing distance from the He atom, the LDOSs of Mo atoms oscillate in a similar manner to the charge density; this result is a strong manifestation of the Friedel oscillation.
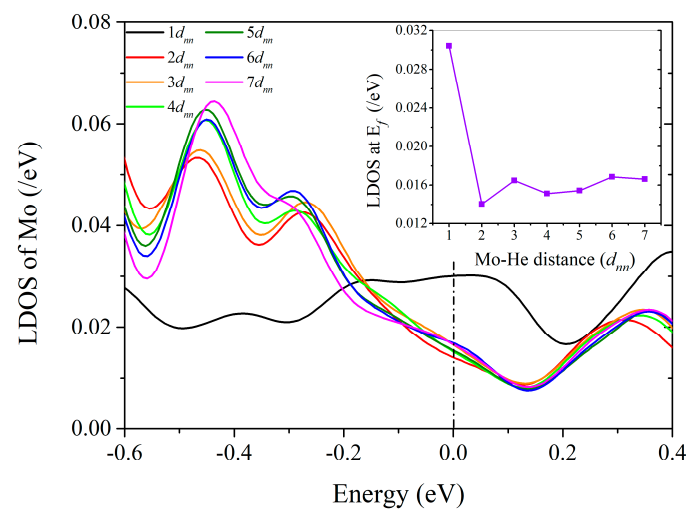

Figure 6. Local densities of states (LDOSs) of Mo atoms in a $(7 \times 7 \times 7)$ supercell of Mo including one substitutional He. The Mo-He direction is along the <111> direction. The Fermi energy is set to zero. The inset displays the LDOSs of different Mo atoms at the Fermi energy level.

Although the charge density oscillations demonstrated in Figure 4 are significant, they do not decay in the form of Equation (2). This is because, unlike s electrons in Mg, d electrons in Mo have remarkable distributions near the atomic core that are not very relevant to chemical bonding. Friedel oscillations involve electronic states near the Fermi energy level, which are distributed mainly in the interstitial region. Therefore, tracking the change in charge density in the nearby interstitial region in the presence of He is more indicative of the Friedel oscillation effect. In Figure 7, we display the calculated charge density in the interstitial region (in the middle of Mo-Mo bonds) as squares and show the result of fitting for the Friedel oscillations, which has the following form

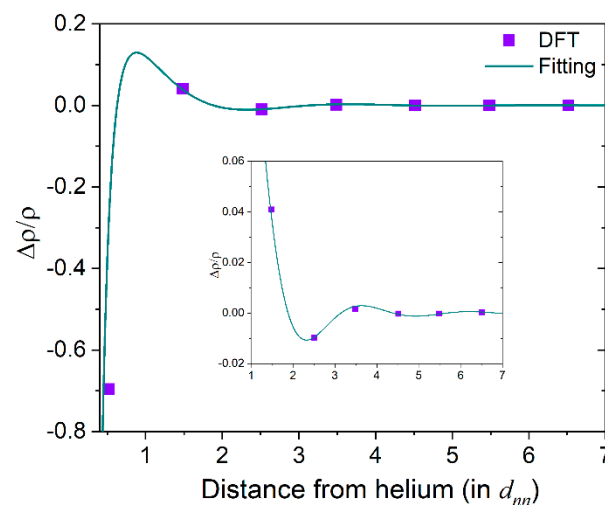$$\frac{\Delta\rho}{\rho} = -0.15 \times \cos(2.5r) \times \frac{1}{r^3}. \tag{3}$$

Figure 7. Fitting of Friedel oscillations of the charge density in the interstitial region in the <111> direction in Mo upon replacing one host atom with a He atom in a ($7 \times 7 \times 7$) Mo supercell.

We note that Equation (2) only holds for large r, so it is not unexpected that the He-induced Friedel oscillations in Mo do not follow the analytical form exactly. The absence of a phase shift is mainly due to the chemical inertness of He, which prevents charge transfer between He and its surrounding atoms. The wavelength of oscillations is approximately 2.5 d_{nn}, which is approximately 6.8 Å smaller than that estimated from the Fermi velocity of Mo (0.92×10^6 m/s), 7.9 Å. The reason for such a discrepancy implies that d electrons in transition metals cannot be described properly by the jellium model as s electrons in simple metals.

4. Concluding Remarks

In summary, we have attempted to clarify if there is a repulsive force between individual He solutes in Mo. Realizing that the size mismatch between He and Mo is marginal and, therefore, the He-He elastic interaction should be very weak, we speculate that it is the He-induced Friedel oscillations of the electron density that produce the potential barriers to hinder the He clustering process. Our first-principles DFT calculations on the solution energies of ordered He atoms, which themselves form a superlattice in Mo, at different concentrations demonstrate that at a high concentration of 3.7 at% (=$1/3^3$), the isomorphic alignment of He (bcc) is energetically more favorable than fcc and simple cubic alignments. Moreover, an even higher concentration of 12.5 at% (=$1/2^3$) proves to be an obstacle for He to merge into clusters. Therefore, Friedel oscillations induced by He atoms modulate He-He interactions in a Mo lattice and provide a thermodynamic driving force to facilitate the alignment of disordered substitutional He atoms into a local Mo-He superlattice at high concentrations. We note that the He atoms can indeed diffuse inside the Mo lattice

with a very small migration energy barrier [28] of 0.06 eV, which helps He atoms find their low-energy alignment quickly. Such local structures might serve as precursors of ordered He bubbles upon the coalescence of individual He atoms.

Friedel had realized, before the advent of electronic computers, that charge density oscillations in metals induced by solute atoms could generate long-range interactions between them, but it is only with the help of high-performance supercomputers that we can precisely evaluate such long-range effects. Our finding in this work suggests that Friedel oscillations can play important roles in the mechanical properties of alloys, beside its well-known effect on electronic properties, such as a Knight shift in the frequency of the nuclear magnetic resonance (NMR) and Ruderman–Kittel–Kasuya–Yosida (RKKY) magnetic interactions in dilute alloys. We might expect the exploration of the Friedel oscillation effects in alloys to deepen our understanding of solute–solute interactions, which govern precipitation and decomposition processes, thereby promoting material innovation.

References

1. Evans, J.H. Observations of a Regular Void Array in High Purity Molybdenum Irradiated with 2MeV Nitrogen Ions. *Nature* **1971**, *229*, 403–404. [CrossRef] [PubMed]
2. Sass, S.L.; Eyre, B.L. Diffraction from Void and Bubble Arrays in Irradiated Molybdenum. *Philos. Mag.* **1973**, *27*, 1447–1453. [CrossRef]
3. Johnson, P.B.; Mazey, D.J. Helium Gas Bubble Lattices in Face-Centred-Cubic Metals. *Nature* **1978**, *276*, 595–596. [CrossRef]
4. Jäger, W.; Trinkaus, H. Defect Ordering in Metals under Irradiation. *J. Nucl. Mater.* **1993**, *205*, 394–410. [CrossRef]
5. Johnson, P.B.; Mazey, D.J. Gas-Bubble Superlattice Formation in Bcc Metals. *J. Nucl. Mater.* **1995**, *218*, 273–288. [CrossRef]
6. Tewary, V.K.; Bullough, R. Theory of the Void Lattice in Molybdenum. *J. Phys. F Met. Phys.* **1972**, *2*, L69–L72. [CrossRef]
7. Stoneham, A.M. Theory of Regular Arrays of Defects: The Void Lattice. *J. Phys. F Met. Phys.* **1971**, *1*, 778–784. [CrossRef]
8. Willis, J.R. The Interaction of Gas Bubbles in an Anisotropic Elastic Solid. *J. Mech. Phys. Solids* **1975**, *23*, 129–138. [CrossRef]
9. Krishan, K. Kinetics of Void-Lattice Formation in Metals. *Nature* **1980**, *287*, 420–421. [CrossRef]
10. Woo, C.H.; Frank, W. A Theory of Void-Lattice Formation. *J. Nucl. Mater.* **1985**, *137*, 7–21. [CrossRef]
11. Ghoniem, N.M.; Walgraef, D.; Zinkle, S.J. Theory and Experiment of Nanostructure Self-Organization in Irradiated Materials. *J. Comput. Mater. Des.* **2001**, *8*, 1–38. [CrossRef]
12. Yu, H.C.; Lu, W. Dynamics of the Self-Assembly of Nanovoids and Nanobubbles in Solids. *Acta Mater.* **2005**, *53*, 1799–1807. [CrossRef]
13. Hu, S.; Burkes, D.E.; Lavender, C.A.; Senor, D.J.; Setyawan, W.; Xu, Z. Formation Mechanism of Gas Bubble Superlattice in UMo Metal Fuels: Phase-Field Modeling Investigation. *J. Nucl. Mater.* **2016**, *479*, 202–215. [CrossRef]
14. Sun, C.; Sprouster, D.J.; Zhang, Y.; Chen, D.; Wang, Y.; Ecker, L.E.; Gan, J. Formation Window of Gas Bubble Superlattice in Molybdenum under Ion Implantation. *Phys. Rev. Mater.* **2019**, *3*, 103607. [CrossRef]
15. Liou, K.-Y.; Smith, H.V.; Wilkes, P.; Kulcinski, G.L. Observations on Ordered Voids in Molybdenum. *J. Nucl. Mater.* **1979**, *83*, 335–339. [CrossRef]

16. Nørskov, J.K. Electronic Structure of H and He in Metal Vacancies. *Solid State Commun.* **1977**, *24*, 691–693. [CrossRef]
17. Seletskaia, T.; Osetsky, Y.; Stoller, R.E.; Stocks, G.M. First-Principles Theory of the Energetics of He Defects in Bcc Transition Metals. *Phys. Rev. B* **2008**, *78*, 1–9. [CrossRef]
18. Inglesfield, J.E.; Pendry, J.B. Energy of Helium Dissolved in Metals. *Philos. Mag.* **1976**, *34*, 205–215. [CrossRef]
19. Jiang, B.; Wan, F.R.; Geng, W.T. Strong Hydrogen Trapping at Helium in Tungsten: Density Functional Theory Calculations. *Phys. Rev. B* **2010**, *81*, 1–8. [CrossRef]
20. Friedel, J. XIV. The Distribution of Electrons Round Impurities in Monovalent Metals, London, Edinburgh. *Dublin Philos. Mag. J. Sci.* **1952**, *43*, 153–189. [CrossRef]
21. Blandin, A.; Friedel, J. Effets Quadrupolaires Dans La Résonance Magnétique Nucléaire Des Alliages Dilués. *J. Phys. Radium* **1960**, *21*, 689–695. [CrossRef]
22. Kresse, G.; Furthmüller, J. Efficient Iterative Schemes for Ab Initio Total-Energy Calculations Using a Plane-Wave Basis Set. *Phys. Rev. B Phys.* **1996**, *54*, 11169–11186. [CrossRef] [PubMed]
23. Blöchl, P.E. Projector Augmented-Wave Method. *Phys. Rev. B* **1994**, *50*, 17953–17979. [CrossRef] [PubMed]
24. Perdew, J.P.; Burke, K.; Ernzerhof, M. Generalized Gradient Approximation Made Simple. *Phys. Rev. Lett.* **1996**, *77*, 3865–3868. [CrossRef] [PubMed]
25. Cao, J.L.; Xie, W.Q.; Lin, J.B.; He, X.F.; Wang, V.; Ogata, S.; Geng, W.T. Off-center positioning of helium in a vacancy in metals. *J. Nucl. Mater.* **2024**, *592*, 154965. [CrossRef]
26. Cho, J.; Zhang, Z.; Plummer, E.W. Oscillatory Lattice Relaxation at Metal Surfaces. *Phys. Rev. B* **1999**, *59*, 1677–1680. [CrossRef]
27. Gall, D. Electron Mean Free Path in Elemental Metals. *J. Appl. Phys.* **2016**, *119*, 1–5. [CrossRef]
28. Cao, J.L.; Geng, W.T. Migration of helium-pair in metals. *J. Nucl. Mater.* **2016**, *478*, 13–25. [CrossRef]